# Precipitation forecasts at the Canadian Meteorological Centre

By DAVID DAVIES and MARVIN P. OLSON, *Atmospheric Environment Service, Montreal, Quebec, Canada*

(Manuscript received July, 7, 1972)

ABSTRACT

Operational forecasts of precipitation amount are produced by a numerical scheme which uses the dew point depression as the moisture parameter. The onset of large scale precipitation occurs gradually when the dew point depression decreases below a threshold value. Small scale precipitation is divided into several meteorological components and each of these is parameterized separately. Improvements were recently obtained by reducing the horizontal grid spacing from 381 km to 190.5 km.

## 1. Introduction

Numerical forecasts of precipitation amount for three layers of the atmosphere have been produced operationally at the Canadian Meteorological Centre (formerly the Central Analysis Office) since February 1968. Although winds and vertical motions have so far been provided by a filtered equations baroclinic model, there are plans to change over to a primitive equations model in the not too distant future. In describing the highlights of the current version of the precipitation scheme in this paper, therefore, it is appropriate to emphasise those general features which appear to be independent of the type of model providing the winds. These are the choice of moisture parameter, the techniques for providing a gradual transition between saturated and unsaturated conditions at grid-points, and the breakdown of precipitation into large scale and small scale components. On the other hand, there are some special features which warrant only a brief coverage here, even though they play an important role in determining the quality of the final product. This is because they were developed solely to compensate for specific inadequacies of the filtered model, such as those arising from the static stability assumptions and the neglect of the divergent part of the wind. The development of the precipitation scheme prior to 1970 is described in the comprehensive technical reports by Davies (1967, 1970). And the main features of the first operational version are given by Kwizak & Davies (1969) and Davies & Olson (1968). However, no particular attempt was made to distinguish between general and special features in any of these earlier publications.

The grid network used for the finite difference calculations is based on a polar stereographic map projection. The grid spacing was originally the standard one of 381 km at 60° N, but recently it was reduced by a factor of two. This increase in resolution was made operationally feasible by decreasing the area of integration and using time-dependent boundary conditions from previous standard grid integrations. The formal change-over of operational procedures from standard grid to fine grid took place on April 15, 1972. Prior to this time, however, both types of forecast had been prepared twice-a-day for four months. This provides an ample basis for commenting on the differences between the fine grid precipitation forecasts and their standard grid counterparts.

## 2. The choice of the moisture parameter

The dew point depression was chosen as the moisture parameter because it provides a direct measure of closeness-to-saturation. This is the grid-point property which is of primary importance for modelling physical processes involving moisture. In particular, the use of the dew point depression avoids the problem of having to compute a derived measure of closeness-to-saturation as a difference between two quantities predicted by more or less independent integration cycles, which may or may not have very different error characteristics. The dew point depression also has other advantages. Because it varies relatively smoothly in the horizontal and in the vertical, at least in comparison to other moisture parameters, it is a suitable variable for use in a three-dimensional numerical advection scheme. And abrupt variations, when they do occur, are not in the middle of critical areas which are close to saturation. Finally, not only is the dew point depression the moisture parameter objectively analysed at the Canadian Meteorological Centre, it is also the one actually reported from radiosonde ascents.

In the formalism the dew point depression will be denoted by the single symbol $S$ (instead of the usual $T - T_d$) to emphasise the fact that it is the primary moisture variable. No distinction will be drawn between the dew point depression and the frost point depression; this is a matter taken care of by the temperature variation of such quantities as the latent heat of vaporization.

## 3. The gradual onset techniques

Physically, the variable $S$ carried in a numerical model must be regarded as some kind of mean value representative of the volume of moist air surrounding a grid-point. However, near saturation at least, there will be local occurrences of cloud and precipitation long before this mean value of $S$ is zero. The actual onset of what would normally be regarded as large scale precipitation somewhere within the area associated with a grid-point will occur when the mean $S$, i.e. the atmospheric value corresponding to the grid-point value of $S$ carried by the model, reaches some *threshold value* $S_1$. If the air has a slight tendency towards static instability, and if it also has moderate horizontal temperature gradients, then it will be prone to strenuous sub-grid scale activity and $S_1$ will be relatively large. On the other hand, if the air is statically very stable, and if it has no horizontal temperature gradients, then it will only exhibit weak sub-grid scale activity and $S_1$ will be relatively small. When the grid-point value of $S$ attains $S_1$, the areal average value of the large scale precipitation rate does not suddenly jump up from zero to the full rate that would be expected at $S = 0$. Instead there will be a gradual increase in rate as $S$ decreases from $S_1$ to 0. The *onset function*, $\chi_1(S)$, is then defined as the ratio of the rate at $S$ to the rate at $S = 0$. Thus $\chi_1(0) = 1$ and $\chi_1(S_1) = 0$; and $0 < \chi_1(S) < 1$ when $S_1 > S > 0$. For convenience, the definition of $\chi_1(S)$ can be extended to all $S \geq 0$ by stipulating that $\chi_1(S) = 0$ when $S > S_1$. Furthermore, $\chi_1$ may depend on quantities other than $S$ and so is more correctly written $\chi_1(S, S_1, \omega, \mathbf{V}, \nabla T, I)$, where $I$ is the Showalter Index. If now the assumption is made that the air already contains as many cloud droplets as it can possibly hold in suspension when $S = 0$, then it follows that the precipitation rate is equal to the condensation rate when $S = 0$. Consequently, the general expression for the large scale precipitation amount is given by

$$\Upsilon_l = \begin{cases} \chi_1 G\left(p, T, \omega, \dfrac{d\tilde{Q}}{dt}\right) \dfrac{\Delta p}{g} \Delta t & \text{if } G > 0 \\ 0 \quad \text{if } G \leq 0 \end{cases} \tag{1}$$

where

$$G = -\left[\frac{F_1(p,T)\,\omega}{p} + \frac{F_2(p,T)}{C_p T}\frac{d\tilde{Q}}{dt}\right] \tag{1 a}$$

$$F_1(p,T) = \frac{r_w \alpha_1}{1 + r_w}\left[\frac{\varepsilon L}{C_p T}\frac{\alpha_2 \alpha_1}{\alpha_3} - 1\right] \tag{1 b}$$

$$F_2(p,T) = r_w \alpha_1 \frac{\varepsilon L}{RT}\frac{1}{\alpha_3} \tag{1 c}$$

$$\alpha_1 = 1 + \frac{r_w}{\varepsilon} \tag{1 d}$$

$$\alpha_2 = 1 + \frac{L r_w}{RT} \tag{1 e}$$

$$\alpha_3 = 1 + b r_w + \frac{r_w}{C_p}\frac{\varepsilon L^2}{RT^2}\alpha_1 \tag{1 f}$$

$$b = \frac{8.064}{7\varepsilon} \tag{1 g}$$

$d\tilde{Q}/dt$ is the heating rate due to effects other than the release of latent heat, $\Delta p$ is the thickness of the layer, $r_w(p, T)$ is the saturated mixing ratio, $L(T)$ is the latent heat of vaporization of water (or ice), $\varepsilon = 0.622$, $\Delta t$ is the time step, and the remaining symbols are standard. The main additional assumptions made in the derivation of (1) are the vertical finite difference approximation for the integral over the layer and the neglect of the liquid water mixing ratio. These two assumptions will usually tend to cancel each other out. In practice it is convenient to express $F_1$ and $F_2$ in tabular form. Furthermore, if the model is using pressure co-ordinates the tables can also include a factor to convert from mass to depth of liquid water, $\Delta t$, $\Delta p/g$ and the denominators of (1a). The idea of using tables for precipitation rate was first suggested by Fulks (1935) and numerical values of the type he advocated were later listed in the Smithsonian Tables (1958). However, the conventional thermodynamic relationships underlying equation (1), and also eq. (2) and (3) which follow, are to some extent based on the material collected together by Godson (1958).

After the large scale precipitation itself, the moisture-related quantity of greatest interest is the large scale heating rate, $dQ_L/dt$, due to the release of latent heat of condensation when clouds and precipitation are formed, and also to the absorption of latent heat when clouds evaporate away. By arguments similar to those used for the large scale precipitation, it can be reasoned that there must exist some threshold dew point depression, $S_2$, at which clouds significant for $dQ_L/dt$ begin to form or finish evaporating away. There must also exist some onset function $\chi_2(S)$ which, for phase changes in the same direction, gives the ratio of the value of $dQ_L/dt$ at any $S$ to that at $S=0$. As before, $\chi_2(0)=1$ and $0<\chi_2(S)<1$ when $S_2>S>0$; and $\chi_2(S)=0$ when $S \geqslant S_2$. It follows that

$$\frac{dQ_L}{dt} = \chi_2 LG\left(p, T, \omega, \frac{d\tilde{Q}}{dt}\right) \tag{2}$$

where $G$ is given by (1a). This equation differs from (1) in that it holds true for negative $G$, i.e. the case when latent heat is absorbed by evaporating clouds. The implication here, of course, is that $\chi_2(S,-\omega)>\chi_2(S,\omega)$ for $\omega>0$ and $0<S<S_2$.

The prediction equation for $S$ is also treated so that there is a gradual transition between saturated and unsaturated conditions. In the fully saturated case $dS/dt=0$. Under moist unsaturated conditions when no clouds are present $dS/dt$ is obtained by subtracting $dT_d/dt$ from the thermodynamic equation, recalling that by definition $T_d=T_d(p,r)$. Let the threshold dew point depression at which clouds significant for $dS/dt$ begin to form be $S_3$, and let the associated onset function appropriate to the change-over from unsaturated cloud-free conditions to the saturated case be $\chi_3(S)$. It follows that in pressure coordinates

$$\frac{\partial S}{\partial t} = -\mathbf{V}\cdot\nabla S - \omega\frac{\partial S}{\partial p} + E(S) + (1-\chi_3)\left\{\left[\frac{RT}{C_p p} - \left.\frac{\partial T_d}{\partial p}\right|_r\right]\omega + \frac{1}{C_p}\frac{d\tilde{Q}}{dt} + \left.\frac{\partial T_d}{\partial r}\right|_p \frac{dr}{dt}\right\} \tag{3}$$

where areal average supersaturation is not allowed, so that $S \geqslant 0$ is enforced everywhere as an over-riding condition, and where

$$\left.\frac{\partial T_d}{\partial p}\right|_r = \left(\left.\frac{\partial T}{\partial p}\right|_{r_w}\right)_{\substack{r_w=r\\T=T_d}} = \frac{RT_d^2}{\varepsilon p L(T_d)} \tag{3 a}$$

$$\left.\frac{\partial T_d}{\partial r}\right|_p = \left(\left.\frac{\partial T}{\partial r_w}\right|_p\right)_{\substack{r_w=r\\T=T_d}} = \frac{\varepsilon p}{r(r+\varepsilon)}\left.\frac{\partial T_d}{\partial p}\right|_r \tag{3 b}$$

$r$ is the mixing ratio of water vapour, and $E(S)$ is an eddy diffusion term. The explicit moisture source term involving $dr/dt$ is needed to account for two types of effect. First, evaporation from the Earth's surface, which in particular prevents the lowest layer becoming excessively dry; and also the reverse process involving condensation. Second, the complete or partial evaporation of precipitation falling through dry layers below the layer in which it originated. These are, of course, all effects which have to be parameterized in some way. In each case the physical consideration of paramount importance will be the closeness-to-saturation. Consequently, it is to be expected that these parameterizations will more naturally feature $S$ rather than $r$. As a corollary, it follows that the latent heat term will have to be corrected to allow for the evaporation of falling precipitation; and, incidentally, also for the changes of phase of falling precipitation.

The gradual onset techniques just described have many advantages. They avoid the undesirable numerical repercussions sometimes associated with the inclusion of on–off effects in a model. They neatly resolve the theoretical ambiguity between condensation and precipitation. They simulate the effects due to the condensation and evaporation of clouds as well as those due to the condensation of precipitation. And they do all these things without requiring cloud mass to be explicitly carried along in the model as an unverifiable intermediate variable. Finally, the fact that three different sets of onset criteria are used means that each can be adjusted separately to optimize the operational performance of the model. The large scale precipitation criteria can be tuned to optimum values by verifying the predicted amounts against those observed. The latent heat criteria can be tuned by verifying the height forecasts against the corresponding objective analyses. And the $S$-equation criteria can be tuned by similarly verifying the predicted $S$ fields.

Historically, the onset techniques have evolved gradually. The first experiments were carried out with a sudden onset at $S_1 = S_2 = 3$. At a very early stage Danard (1964, 1966*a*, 1966*b*) suggested the use of linear onset functions. Consequently, these were made a feature of the first operational model when $\omega < 0$; they were used in conjunction with $S_1 = S_2 = S_3 = (7.5 - 0.052\ t)$ °C where $t$ was the time in hours from the beginning of the forecast period. Later, a linear $\chi_3$ was applied when $\omega < 0$ because this was found to improve the verification scores of the predicted $S$ fields. During the operational lifetime of the standard grid model several minor adjustments were made to the $S_n$ and $\chi_n$ at particular grid-points to overcome specific deficiencies of the precipitation forecasts. At the time these were considered to be technical expediencies rather than scientific innovations. Meanwhile some experiments with latent heat feedback in the filtered model by Davies (1970) had indicated that $(S_1, \chi_1)$ and $(S_2, \chi_2)$ should be different. Once again this appeared under the guise of technical expediency. However, these two apparently unrelated technical developments, taken together, were the forerunner of a major evolution in design which took place with the advent of the fine grid model.

The first fine grid experiments involving moisture took place in the autumn of 1971. The resulting precipitation forecasts looked more realistic than their standard grid counterparts. But they did not verify quite as well. This was because of the heavy penalties attached to displacement errors when the forecasts become more detailed. The vast majority of all errors were attributable to errors in the predicted wind fields. However, a thorough examination of many cases revealed that some errors were not due to the wind fields. These errors showed up quite clearly on the fine grid forecasts because they usually extended over six to fourteen grid-points. But errors covering the same areas were almost impossible to detect on the standard grid forecasts without knowing where to look for them. This was because they usually involved only one to three grid-points on the edge of a much larger precipitation region. Once such errors were detected, it was not difficult to diagnose their source as the crudity of the onset procedures. Further experimentation led to the development of fully variable onset procedures. At present, $S_1$ is given by

$$S_1 = \frac{(4+\beta_1)(30-I^*)\beta_2}{96} S_0 \tag{4}$$

where

$$\beta_1 = \begin{cases} 2 & \beta_1^* > 2 \\ \beta_1^* & 0 \leqslant \beta_1^* \leqslant 2 \\ 0 & \beta_1^* < 0 \end{cases} \tag{4 a}$$

$$\beta_1^* = a_1(\nabla T)^2 + a_2(\mathbf{V}\,\nabla T) \tag{4 b}$$

$$I^* = \begin{cases} 12 & I > 12 \\ I & 0 \leqslant I \leqslant 12 \\ 0 & I < 0 \end{cases} \tag{4 c}$$

$I$ is again the Showalter Index, $a_1$ and $a_2$ are slowly varying functions of $T$, and $\beta_2(p, p_g)$ is a correction factor to be applied over mountain plateaus of pressure-height $p_g$. The complementary onset functions $\chi_1$ consist of a set of essentially bell-shaped curves which are currently constructed by joining two parabolic segments together in the following manner:

$$\chi_1 = \begin{cases} 1 + \dfrac{S_1^*}{S_1}\left(\dfrac{S_1^*}{S_1}X - 1 - X\right)\left(\dfrac{S}{S_1^*}\right)^2 & \text{if } 0 \leqslant S < S_1^* \\ 1 - (1+X)\dfrac{S}{S_1} + X\left(\dfrac{S}{S_1}\right)^2 & \text{if } S_1 > S \geqslant S_1^* \\ 0 \quad \text{if } S \geqslant S_1 \end{cases} \tag{5}$$

where

$$X = X_\omega X_S \tag{5 a}$$

$$S_1^* = \left[\frac{S_0}{2} + J\left(S_1 - \frac{S_0}{2} - 0.1\right)\right][X_\omega^4 + (1 - X_\omega^4)J] \tag{5 b}$$

$$X_\omega = \begin{cases} \dfrac{\omega_X - |\omega|}{\omega_X} & \text{if } |\omega| < \omega_X \\ 0 & \text{if } |\omega| \geqslant \omega_X \end{cases} \tag{5 c}$$

$$X_S = \begin{cases} 1 & \text{if } S_1 \geqslant S_0 \\ 4\left(\dfrac{S_1}{S_0} - 0.75\right) & \text{if } 0.75\,S_0 < S_1 < S_0 \\ 0 & \text{if } S_1 < 0.75\,S_0 \end{cases} \tag{5 d}$$

$$J = \begin{cases} 1 & \text{if } I \leqslant -3 \\ \dfrac{3-I}{6} & \text{if } 3 > I > -3 \\ 0 & \text{if } I \geqslant 3 \end{cases} \tag{5 e}$$

$\omega_X$ has a slight dependence on $T$, and $S_0$ is 7°C initially and slowly decreases with time. The unwieldy formulations (4) and (5) may be lacking in elegance, but they simulate the onset of large scale precipitation in a much more realistic fashion than their predecessors.

## 4. The small scale precipitation

The large scale precipitation amounts predicted by the methods of the last Section fail to correspond to the observed precipitation patterns in one very important respect. The showery or small scale precipitation associated with convective cloud cells is either missed completely or grossly underforecast. It is clear that, with current computing power, this deficiency can only be overcome by resorting to some kind of parameterization. The procedure that has actually been adopted may be generalized as follows.

Let the areal average or grid-point value of the small scale precipitation amount originating from a given layer in time $\Delta t$ be $\Upsilon_s$. Suppose that $\Upsilon_s$ can be broken down into $n$ meteorological components, $\Upsilon_{si}$, $i = 1, 2, ..., n$, such that the $i$th component has associated with it a *scaling factor* $A_i$ and $J_i$ *characteristic variables* $\eta_{ij}$ together with complementary *threshold values* $\eta_{ij}^*$ and *onset functions* $\chi_{ij}(\eta_{ij} - \eta_{ij}^*)$, $j = 1, 2, ..., J_i$. Then

$$\Upsilon_s = \sum_{i=1}^{i=n} \Upsilon_{si} = \frac{F_1(p, T)}{p}\frac{\Delta p}{g}\Delta t \times \sum_{i=1}^{i=n} A_i \prod_{j=1}^{j=J_i} \chi_{ij}(\eta_{ij} - \eta_{ij}^*) \tag{6}$$

where $F_1$ is given by (1b). An onset function is defined to be zero when its characteristic variable does not satisfy its threshold condition; thus $\Upsilon_{si}$ is zero if any one of its characteristic variables fails to attain its threshold value.

The breakdown of $\Upsilon_s$ into components, the evaluation of the scaling factors $A_i$, and the assignment of characteristic variables $\eta_{ij}$, thresholds $\eta_{ij}^*$ and onsetf unctions $\chi_{ij}$ have so far been done solely by trial and error on the basis of meteorological experience. This completely empirical approach has been pragmatically justified in two ways. First, the objective of predicting shower activity has been successfully attained. Most errors that do occur can be attributed to errors in the forecast of the large scale flow. Second, the resources devoted to work on the small scale precipitation problem have been kept down to about 20% of those allotted to the entire precipitation scheme. Note that the general form of the parameterization formula (6) has been established without having to resort to a detailed modelling of arrays of convective elements. In any case, even if an array model of convection were to lead to the breakdown of small scale precipitation into components with associated sets of $A_i$, $\eta_{ij}$, $\eta_{ij}^*$ and $\chi_{ij}$, the precise numerical values needed for the incorporation of these quantities into an operational program would still have to be determined empirically. The only question such an array model might conceivably answer would be whether the empirically derived formulations are complete and in their most convenient form. Unfortunately, this aspect is not independent of the characteristics of the model providing the winds, since such things as the physical assumptions and the mathematical approximations must certainly be taken into account, so even here the ultimate rationale must be largely empirical.

At the time of writing the small scale parameterization formulae are undergoing a thorough re-appraisal in preparation for their incorporation into the primitive equations model.

In particular, an attempt is being made to introduce variable threshold criteria in a more systematic fashion than at present. Briefly, the thresholds for small scale precipitation have been undergoing an evolution similar to those reported for large scale precipitation in the last Section. Originally, constant threshold values were used everywhere. These were subsequently amended in piecemeal fashion to overcome specific deficiencies in the forecasts. Consequently, they have now reached a somewhat untidy state mid-way between technical expediency and scientific innovation. Nevertheless, in view of the current interest in parameterization, a slightly simplified presentation of some of the details of the current formulae is not out of place here.

Some problems are common to all of the meteorological components into which small scale precipitation is broken down. For instance, since the total amount of moisture available over any grid square is strictly limited, the $\chi_{ij}$ should strictly speaking be dependent on the sum of $(\Upsilon_l + \Upsilon_s)$ over all the layers. This presents a difficulty as one needs to know $\Upsilon_s$ before it has been computed. In practice, therefore, this dependence has so far been accomplished by computing a value $\hat{\Upsilon}_s$ from (6) assuming no moisture limitation, and then incorporating a single multiplier dependent on $(\Upsilon_l + \hat{\Upsilon}_s)$, and also on $F_1$, into all the $A_i$. It is also clear that the vertical development of convective clouds through more than one layer should somehow enhance the $\Upsilon_{si}$ values computed for the individual layers. However, this kind of reinforcement effect has not yet been included explicitly because of programming considerations, and also because it seems to be partly taken care of implicitly by the current formulae. Unfortunately, the errors in small scale precipitation forecasts tend to increase more rapidly with time than is the case for large scale precipitation forecasts. This happens because the parameterization (6) is of necessity highly sensitive to errors in the large scale flow patterns. Consequently, the strategy of the situation demands that lesser amounts of small scale precipitation are predicted as time increases. Accordingly, all the $A_i$ are deemed to decay a percentage point or so per hour, and similar adjustments are made to some of the threshold values $\eta^*_{ij}$.

The three meteorological components of small scale precipitation which have been identified so far are: (i) frontal showers, (ii) air mass showers, (iii) induced showers. Assigning $i = 1, 2, 3$ to these in order, the characteristic variables of eq. (6), with $n = 3$, $J_1 = J_2 = 5$, and $J_3 = 2$, are given by:

$$\eta_{11} = (\nabla T)^2, \quad \eta_{12} = |\mathbf{V} \cdot \nabla T|, \quad \eta_{13} = \hat{\mathbf{k}} \cdot \nabla \mathbf{x} \mathbf{V},$$
$$\eta_{14} = \eta_{24} = -S, \quad \eta_{15} = \eta_{25} = -\omega, \quad \eta_{21} = \eta_{31} = -I,$$
$$\eta_{22} = -\eta_{23} = t_a, \quad \eta_{32} = \Upsilon_l + \Upsilon_{s1} \tag{6a}$$

where the signs have been chosen so as to make $(\eta_{ij} - \eta^*_{ij})$ positive when the threshold condition for occurrence is satisfied, and $t_a$ is the local time-of-day. So far a zero value has been assigned to $\eta^*_{12}$, $\eta^*_{13}$ and $\eta^*_{32}$; noon to $\eta^*_{22}$ and midnight to $(-\eta^*_{23})$; and Showalter Index values of 3 at low levels to 2 at 500 mb to $(-\eta^*_{21})$ and $(-\eta^*_{31})$. The vertical motion thresholds $(-\eta^*_{15})$ and $(-\eta^*_{25})$ are variable and allow showers with slight subsidence. The dew point depression thresholds $(-\eta^*_{14})$ and $(-\eta^*_{24})$ are also variable and are set at a slightly higher value than their counterpart $S_1$ for the onset of large scale precipitation. Finally, $\eta^*_{11}$ is variable with level and to some extent with temperature. Excluding the overall moisture limitation multiplier which has been combined with the $A_i$, the onset functions $\chi_{ij}$ are all simply $(\eta_{ij} - \eta^*_{ij})$ except as noted in the following remarks. The onset function $\chi_{21}$ is given by $(\eta_{21} - \eta^*_{21})^2$ and $\chi_{31}$ is similar. The onset function $\chi_{13}$, which is associated with the vorticity, acts essentially as a sharp on–off switch at threshold, although it also features a linear increase thereafter. The onset function $\chi_{12}$ acts as a gradual (linear) on–off switch which plays no further role once a fairly modest flow perpendicular to the front is attained; this allows a strong front to be inactive when there is no cross flow, but suddenly come alive with vigorous showers when a slight cross flow is predicted to develop. The two time-of-day contributions taken together merely ensure that air mass showers have a parabolic profile between noon and midnight, with a maximum at 6 p.m. This is the type of constraint that will presumably disappear when solar radiation effects are successfully simulated by the model, but nevertheless serves a vital role in the interim. The foregoing description of the small scale precipitation formulae omits numerical data and some of the more mundane correction factors. For the standard grid this information is given by Davies (1967, 1970).

The corresponding fine grid information will be published in a technical report now under preparation.

As mentioned in the last Section, some experiments with latent heat feedback were done with the filtered model by Davies (1970). When the latent heat was computed from the large scale precipitation alone the resulting forecasts were quite meaningful. However, when the same cases were rerun including the latent heat computed from the small scale precipitation, as well as that from the large scale precipitation, the results were catastrophic. Spurious lows appeared in regions of small scale precipitation. These dutifully generated their own large scale precipitation, and the subsequent developments from the combined latent heat effects took place with quite unmeteorological rapidity. The same kind of phenomena occurred when the small scale latent heat amounts were arbitrarily reduced to 10% of their actual value. It can therefore be inferred that the latent heat released by convective precipitation drives the small scale circulation only, and does not directly affect the large scale flow. Consequently, it appears that the latent heat associated with parameterized small scale precipitation should be discounted altogether in the main model.

It remains to comment on the implications of small scale precipitation for the predictive equation for dew point depression. Convective clouds are known to transport moisture upwards. Consequently, the operational scheme contains a crude mechanism for injecting a small amount of moisture into the 500 mb layer when small scale precipitation is present.

## 5. Special features for the filtered model

The procedures just described can only be used to predict precipitation amount if winds, vertical motions and temperatures are made available as required. In the current operational scheme rather elaborate methods have had to be employed to wrest this information from the filtered model. However, as these methods will soon be rendered obsolete by the changeover to a primitive equations model, a concise description of their main features will suffice here.

The filtered model itself is based on the potential vorticity equation. It includes the eddy diffusion of potential vorticity, a term to control long wave retrogression, and the effects of mountains and surface friction. The operational version has always carried stream function information at the main working levels of 850, 500 and 200 mb, and also at the derived field levels of 700 and 1 000 mb. The development work on the standard grid model was undertaken first by Robert (1963) and then later by Davies & Olson (1968); a full history is given by Davies (1970). The development work on the fine grid model was carried out by Paulin & Olson (1972), following some preliminary experiments by Harvey (1969).

The first of the required variables not directly available is the vertical motion. At 700 and 500 mb the "dry" vertical motion, $\omega_d$, is computed from a simplified version of the thermodynamic equation which assumes that the height can be replaced by the stream function, that the advection of thickness by the divergent part of the wind can be disregarded, that the heat term can be ignored, and that sub-grid scale processes can be simulated by an eddy diffusion term. There is some advantage in evaluating the advection of thickness term with a second order finite difference Jacobian, even though the filtered model itself uses a fourth order scheme for the advection of potential vorticity. The 700 mb stream function can be used in these calculations because it is derived by interpolation. An 850 mb value of $\omega_d$ cannot be computed in the same way because the 1 000 mb stream function is derived by extrapolation and therefore exhibits some phasing peculiarities near low centres; an adjusted 700 mb value of $\omega_d$ has to be used instead. Some proportion of the terrain-induced vertical motion has to be reintroduced explicitly into the $\omega_d$ calculations at all levels because the important short wavelength components of this quantity are unduly suppressed by the finite difference computations. When large scale precipitation is occurring, the "wet" vertical motions, $\omega$, are in principle obtained by adding a heat term to the thermodynamic equation and rewriting it in the form

$$\omega = \frac{\sigma}{\sigma - H}\,\omega_d \tag{7}$$

where $H$ is directly proportional to the amount of large scale latent heat released, and $\sigma$ is the static stability. The quantity $\sigma f_0/f$, which is taken to be dependent only on pressure in the filtered model, is in (7) assumed to vary between the static stability of the standard atmosphere and that of an arbitrary rainy atmosphere which is itself dependent on temperature; here $f$ is the Coriolis parameter and $f_0$ its value at 45° N. Both $\sigma$ and H therefore have some dependence on the threshold $S_2$ and the onset function $\chi_2$ of Section 3. The final value of $\omega$ is strictly limited by the imposition of a complicated system of overall constraints on the amplification of $\omega_d$. The operational $\omega$ forecasts obtained by this method were automatically monitored for a year on the standard grid. In winter the maximum ascent values in the first hour vertical motion fields at 700 mb were about $-32$ mb/hour on an average day; this figure was doubled on an active day, and halved on a quiet day. The corresponding summer figures were half the winter values. Usually the vertical motions at 850 and 500 mb were 70–90% of those at 700 mb. The general tendency was for the first hour magnitudes of the vertical motion fields to decay at 0.5% per hour; though, of course, this effect is masked by synoptic developments in individual cases. No long term monitoring of the magnitude of the fine grid vertical motions has yet been carried out, but the evidence so far suggests they are about 10% or so higher than their standard grid counterparts. The main reason the difference is not greater is that $\omega$ is obtained from the thermodynamic equation and not from the divergence by vertical integration. In addition the many arbitrary constants were retuned for the fine grid scheme and these changes probably led to reductions of 10% or so in the computed values.

The second of the required variables not directly available from the stream function fields of the filtered model is the temperature. Solution of the reverse balance equation by iteration at every time step would be relatively costly in computer time, and might involve some difficulty with the vertical boundary conditions. Consequently, explicit predictions of temperature are obtained by doing time integrations of an appropriate form of the thermodynamic equation which includes an eddy diffusion term. Horizontal advections are computed from the stream function winds. And those terms involving the vertical motion, including the one dealing with release of latent heat, are selectively damped according to the magnitude of $\omega$. Radiation effects are simulated by a specially developed formulization which takes cloudiness and surface exchanges into account. And ocean heating is also handled empirically. The resulting charts of forecast temperature are of excellent quality, though frontal gradients get smoothed out. The largest errors are clearly attributable to incorrect flow patterns from the filtered model.

Advections by the divergent part of the wind have never been computed in the operational model. However, these terms were not neglected in some of the experimental integrations. The results indicated that the divergent part of the wind is highly scale-dependent, and of greatest magnitude in developing cyclones at low levels. Unfortunately, problems arose because meaningful values of velocity potential were very difficult to compute in the most important places.

## 6. Operational aspects

One of the principal objectives of the operational procedures is to transmit fine grid forecasts of precipitation amount to the field offices at about 3 hours after observation time. Since these forecasts are only required for Canada and adjacent regions, they are produced by doing the fine grid integrations over a limited area. Systems moving into this limited area from outside the boundary are treated realistically by supplying time-dependent boundary conditions from earlier standard grid integrations over a larger area. This requires two sets of integration runs to be scheduled for each upper air observation time. The most important of these is the production run which is based on the early transmissions of radiosonde data up to 500 mb from the North American reporting stations, i.e. the so-called RADAT data, and commences 90 minutes after observation time. The other is the mop up run which is based on the complete radiosonde transmissions for the whole northern hemisphere, and begins about 8½ hours after observation time.

In the mop up run the filtered equations model is integrated over a hemispheric standard grid of 2 805 points ($51 \times 55$) to provide predicted boundary conditions for the Laplacian and tendency of the stream function fields. These are required in the next production run for a second standard grid integration of the same model over an intermediate limited area of

1 221 points ($37 \times 33$). This in turn provides the same kind of boundary information for the integration of the fine grid filtered equations model over a smaller limited area of 323 standard grid points ($19 \times 17$)—i.e. 1 221 fine grid points ($37 \times 33$)—which just covers North America. The fine grid precipitation scheme is integrated over the same North American limited area in the production run. In this case, however, boundary conditions for the tendencies of both temperature and dew point depression are predicted by an integration of the standard grid precipitation scheme over the intermediate limited area in the previous mop up run. The standard grid integration of the filtered model over the intermediate area is needed in the production run to meet commitments to provide up-to-date flow pattern predictions over the Atlantic and Pacific Oceans.

The integrations of the filtered equations model are completed right out to the end of the forecast period before the associated integrations of the precipitation scheme commence. The linkage between the two sets of programs is provided by stream function and terrain vertical motion fields which are laid down on disk every time step by the filtered model. This makes the use of computer core storage more efficient than it would otherwise be.

To speed up the fine grid integrations the vertical motion and precipitation computations are computed only at alternate time steps, i.e. every hour instead of every half-hour. For the same reason the threshold $S_1$, the Showalter Index, the radiation term and the ocean heating term are computed only once every $2\frac{1}{2}$ hours. Tests indicated that the resulting forecasts differ only slightly from those for which all quantities are computed every half-hour.

Initial time height, temperature and dew point depression fields for the standard grid are —with one exception—provided by the application of the objective analysis procedures described by Kruger (1965, 1969) and Kruger & Asselin (1967). The exception is the 200 mb height field which is needed for the production run before any 200 mb reports are received. In this case, therefore, the 12-hour 200 mb height forecast produced by the 6-level primitive equations model at the National Meteorological Center, Washington, is used as the initial time chart. This is specially transmitted to Montreal via teletype; when there are communications problems the corresponding 12-hour forecast from the filtered model serves as a substitute. Initial time stream function fields are always obtained from the height fields by solving the balance equation over the whole hemisphere and then extracting the sub-area required; the technique developed by Asselin (1967) is used for this purpose. The initial time charts for the fine grid are obtained from their standard grid counterparts by cubical interpolation.

During the pseudo-operational testing of the fine grid models the standard grid precipitation scheme was integrated both in the production run and in the mop up run for a period of several months. On the average, the precipitation forecasts from the mop up run verified slightly better than those from the production run. Since the differences were usually small, this justifies the use of a 12-hour forecast of the 200 mb height field as an initial time chart in the production run. Nevertheless, there are occasions when the predicted amounts of small scale precipitation are adversely affected by the inaccurate phasing of a 200 mb trough position at initial time.

Objective verifications are routinely carried out by computing threat scores—i.e. "hits"/("forecast" + "observed" − "hits") × 100%— of the station values obtained by interpolation from the precipitation forecasts against the corresponding observed values. Unfortunately, quoted threat scores have no absolute meaning because they vary considerably according to: the time period; the area covered; the amount of precipitation deemed significant; the amount of detail in the forecasts; the quality control measures taken to ensure correct observed data; the proportion of observed precipitation which is convective; and the actual occurrence of observed precipitation. Nevertheless, they do provide an objective means of assessing the relative worth of different forecast models integrated under identical conditions over the same series of cases. Major improvements in the precipitation scheme, such as those obtained by increasing the vertical resolution from one to three layers, or by adding small scale effects in summer, will then give increases in the threat scores which have a high degree of statistical significance. Normally, however, the improvements are minor ones suggested by case studies and the threat score is not a sufficiently precise tool to assess their worth on an individual basis. Then one has to be content with showing that a group of several minor improvements, taken collectively, leads to significant increases in the threat scores.

## 7. Improvements in fine grid forecasts

In general, the fine grid stream function forecasts look remarkably similar to their standard grid counterparts. The main improvement is simply that short wave systems are advected a little faster due to the reduction in truncation error. Occasionally, however, two neighbouring low centres on the initial time charts are resolved into separate entities by the fine grid model, but merged together into one broad trough by the standard grid model. Even when this happens the fine grid forecasts usually bear a fairly close resemblance to the standard grid forecasts. Under exceptional circumstances, however, one of the two lows resolved by the fine grid model undergoes a rapid development while the broad trough seen by the standard grid model does not. The stream function forecasts for the fine grid then differ spectacularly from those for the standard grid. Though only three or four really clearcut cases of this type have so far been encountered, in each and every one of them the fine grid model has successfully simulated a rapid development in the real atmosphere which was missed by the standard grid model.

The differences between the precipitation forecasts for the fine grid and their standard grid counterparts are much more marked than in the case of the stream function forecasts. In particular, the precipitation patterns forecast for the fine grid exhibit much more detail than those forecast for the standard grid. To some degree, of course, this greater detail arises simply because all computations are done with fine grid resolution. This is especially true for orographic precipitation because the mountain field itself can be depicted much more accurately over the fine grid. In addition, as reported in Sections 3 and 4, the variable threshold criteria and more sophisticated onset functions used to predict both large and small scale precipitation in the fine grid scheme also contribute to the increase in detail. Some of the differences in the precipitation charts arise directly from the improvements in the stream function forecasts. The maxima of the precipitation patterns associated with moving single-centred lows are invariably displaced in the direction of the flow by the fine grid scheme. And when developments of multiple centres do take place in a different manner in the fine grid model, these usually lead to the prediction of different maximum values for the centres of the precipitation areas, and sometimes to significant displacements as well. It should be re-emphasised here that in general the maximum values predicted for precipitation areas in the fine grid are only slightly higher than those predicted for corresponding areas in the standard grid. And these slight increases in the fine grid maxima are more than compensated for by the fact they have sharper peaks. As mentioned in Section 5, one reason for this similarity is that the arbitrary constants of both precipitation schemes have been carefully tuned by matching the forecast charts to the observed charts.

The differences in the fine grid precipitation forecasts led to a small increase in the average 24-hour threat scores from January to April 1972. This was the period when both schemes were integrated routinely in the production run. Taken collectively, therefore, the differences are definitely improvements. That each of the differences is also an improvement on an individual basis is evident from the large number of case studies which have been carried out. An example will serve to illustrate how these are done. Fig. 1 gives an objective analysis of the observed precipitation amount over the fine grid for the 24-hour period beginning OOZ, 25th January 1972; no data areas are left blank. For the same initial time, the 24-hour forecast chart for the fine grid is given in Fig. 2, and the corresponding chart for the standard grid in Fig. 3. On all charts contour lines are drawn for 0.01, 0.25, 0.50 and 1.00 inches of rain. On both forecast charts the main precipitation maximum is associated with a low moving northeastward out from the Great Lakes. But whereas the standard grid chart has this maximum south of James Bay, the fine grid model has it east of James Bay. This is due to the greater advection speeds in the fine grid model. It is typical of the type of effect one obtains when dealing with lows with a single centre. Unfortunately, in the real atmosphere a secondary low developed during the forecast period and by OOZ on January 26th this had taken over as the main source of pre-

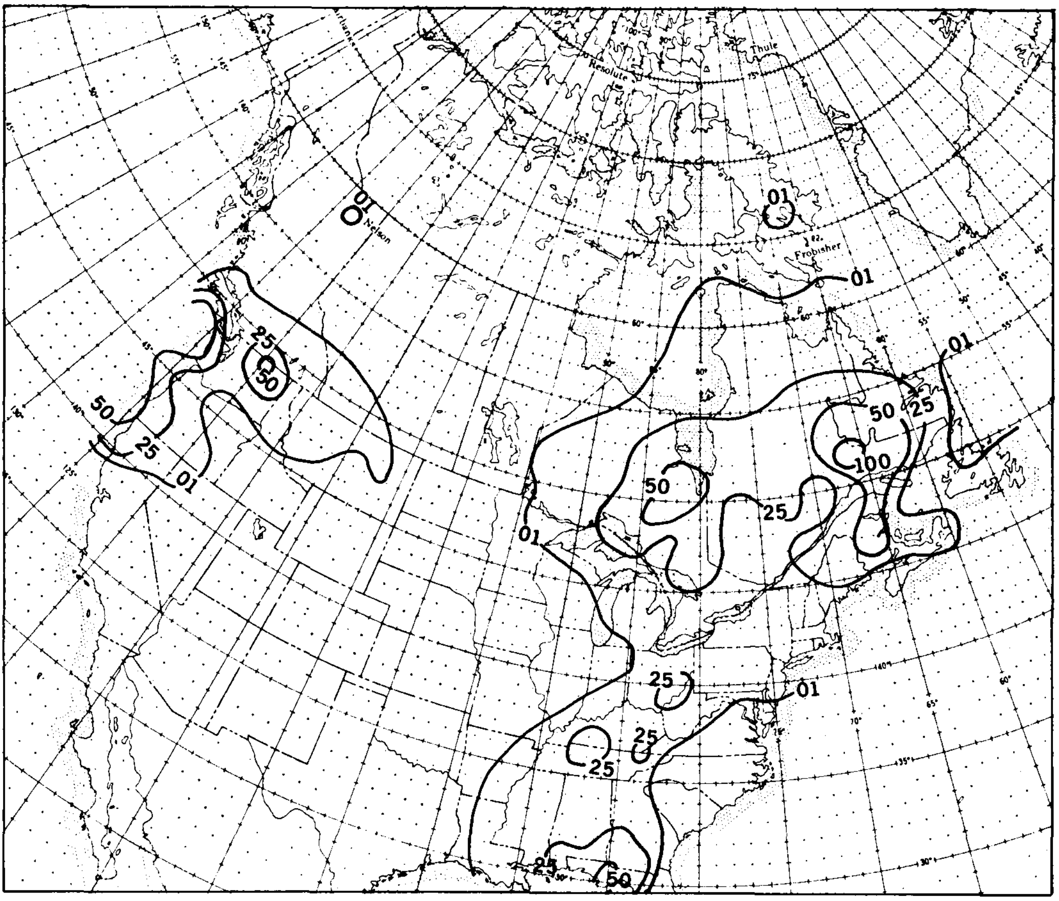


*Fig. 1.* A fine grid objective analysis of the observed precipitation amounts reported in inches for the 24-hour period commencing OOZ, 25th January 1972.

cipitation over the Gulf of St. Lawrence. The original low occluded and slowed down near James Bay. These developments are reflected in the observed chart. The picture in the region is further complicated by the large amounts of snow which fell just north of the Gulf due to the passage of cold air over open water. Neither model caught the secondary low, and no attempt has yet been made to simulate local effects, so both forecasts are somewhat less than perfect. Nevertheless, both models correctly predicted that Ontario, Quebec and the N. E. States would have precipitation that day, and so the forecasts must be judged successful to some degree. A second interesting feature is the precipitation area on the West Coast. In the northern portions the details of the fine grid forecast tally very well with what was observed; the corresponding standard grid forecast, though essentially correct, is just a broad smear. This is an improvement which is due directly to the fine grid mountain field. The southern lobe of the observed pattern was not really caught by either forecast. In spite of the proximity of the fine grid boundary, this was due to the initial time objective analysis over the standard grid being slightly in error over the Pacific. The eastern arm which extends quite far on both forecasts is considerably foreshortened on the observed chart. This error is connected with the failure of the models to occlude the James Bay low. One small error which appears on the forecast for the standard grid but not on that for the fine grid is the minor bump over northern Utah. This is a very modest example of the kind of adjustment which often results

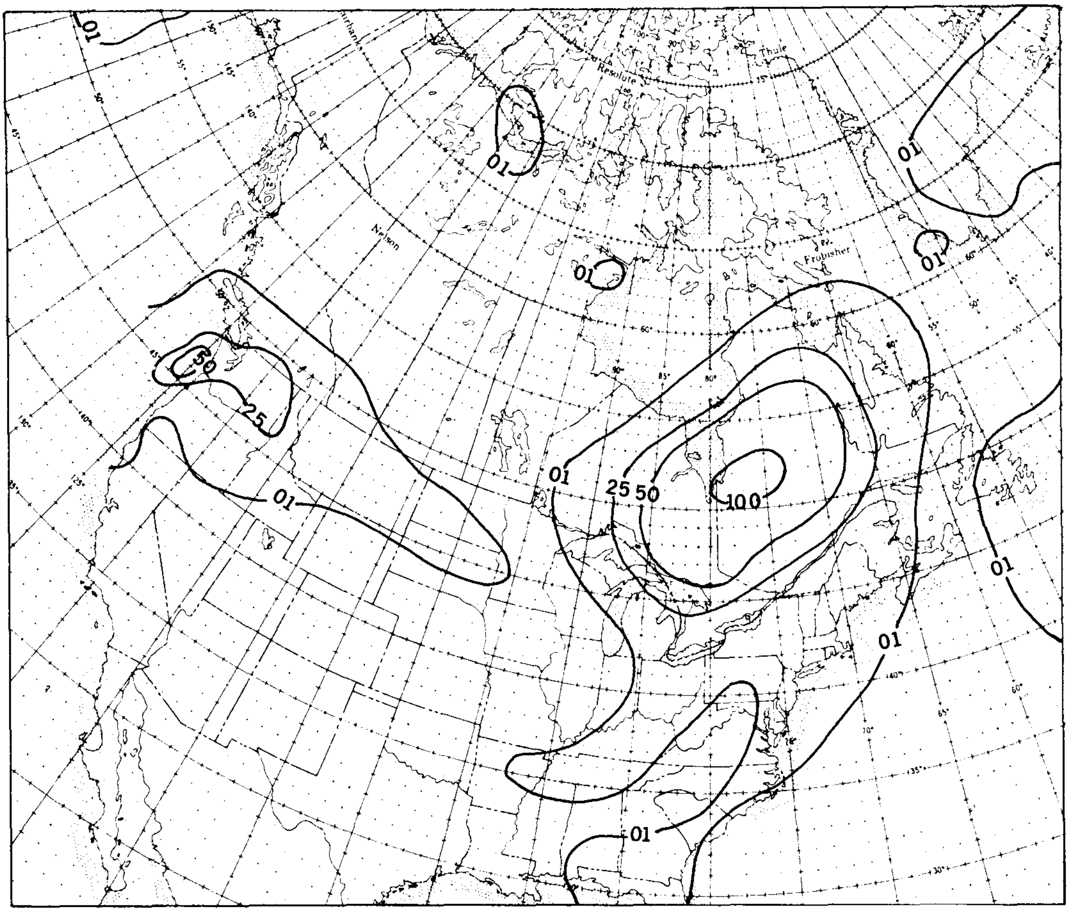

*Fig. 2.* A fine grid forecast of 24-hour precipitation amount in inches from the initial time of OOZ, 25th January 1972.

from the switch-over to variable thresholds and more complex onset functions. The third major area of interest is the S.E. US. From the observed chart it is clear that some small disturbance moved inland from the no data area over the Gulf of Mexico. Something was caught on both forecast charts, but with nowhere near the right intensity. Consequently, the fine grid scheme suffers because it was able to resolve the predicted precipitation pattern into two separate features. Needless to say, neither model moved the cold front against the Appalachian Mountains with sufficient vigour, so the associated precipitation was underforecast. Although the two forecasts and the analysis all show some isolated spots of very light snow in Northern Canada, there is no correlation whatsoever between what was predicted and what was observed. It appears to be almost impossible to predict isolated flurries of this kind with any accuracy. As will now be apparent, this particular case was selected for publication because it enables several different interesting features to be displayed on one set of charts.

This Section will be concluded with a few remarks on precipitation type. The distinction between snow and rain is made according as to whether the 850 mb temperature is greater or less than some critical figure; the actual value varies between 0°C and $-3$°C depending on whether or not there is climatological snow cover. This technique works out very well in practice, both on the standard grid and on the fine grid. Indeed, since the main errors arise

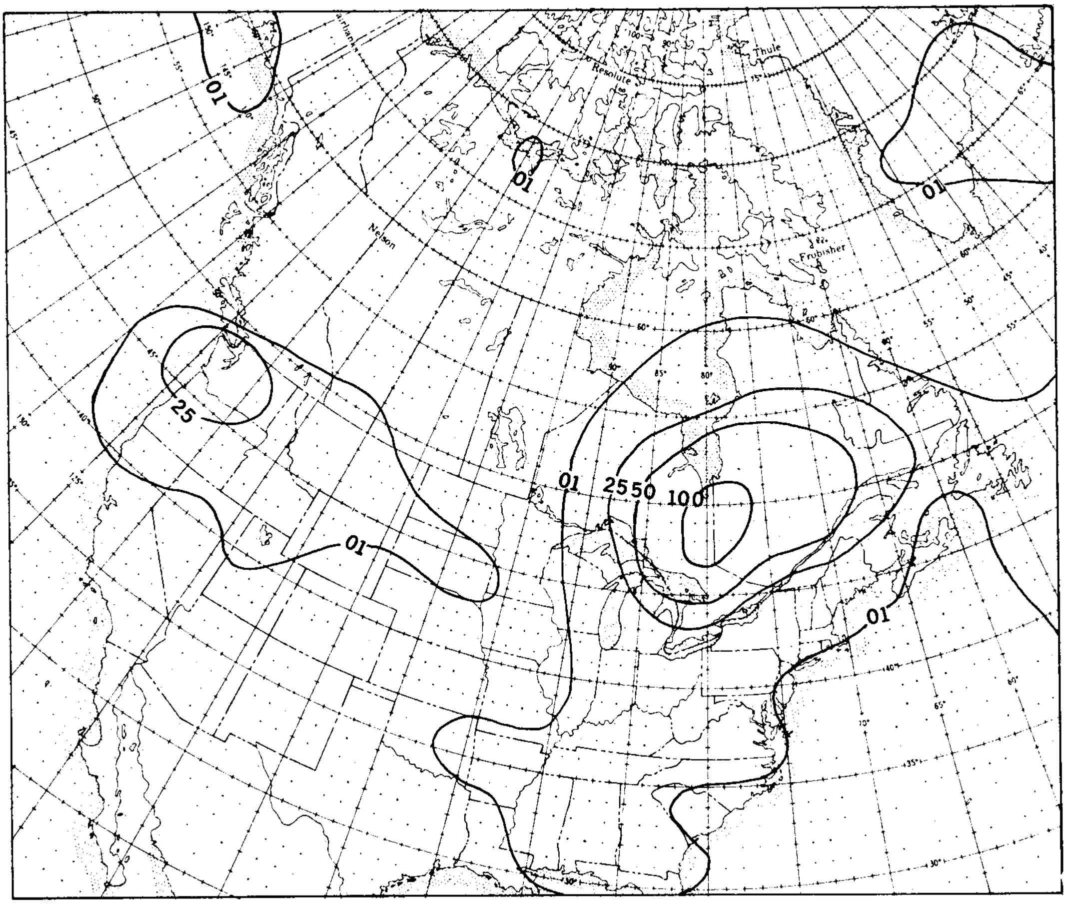


*Fig. 3.* A standard grid forecast of 24-hour precipitation amount in inches from the initial time of OOZ, 25th January 1972.

when the actual snow cover is different from climatology, an attempt will shortly be made to do an objective analysis of snow cover. Similarly, the standard grid scheme has a programmed capability to predict freezing rain when the 700 mb temperature is warmer than 0°C and the 850 mb temperature is cool enough for snow. But in the $4\frac{1}{2}$ years the standard grid scheme has been in operational use it has never once predicted any freezing rain. Consequently, this "sudden onset" switch was modified to a "gradual onset" technique in the fine grid scheme. The proportion of the total amount of precipitation falling as freezing rain is deemed to first become non-zero when the 700 mb temperature warms up above −3°C, and then rise linearly to unity at 0°C. Similarly, ice pellets are predicted when the 850 mb temperature becomes sufficiently cold. This gradual onset technique was an immediate success and the fine grid forecasts of freezing rain and ice pellets now correspond reasonably well to the observed occurrences.

## 8. Future work

The immediate objective is to make the precipitation scheme fully compatible with the primitive equations model developed by Robert et al. (1972) following some earlier work on a semi-implicit time integration scheme by Kwizak & Robert (1971). This will involve doing studies on the quality of the wind, vertical motion, and temperature forecasts that are to be provided in order to diagnose and eliminate any systematic deficiencies of the type that were originally encountered with the filtered equations model. Both the horizontal and vertical resolution will be increased still further when more computing power is made available. This implies that some attention will have to be given to the problem of providing initial time charts for high resolution integrations. Meanwhile, the division of small scale precipitation into meteorological components with associated characteristic functions, and the procedures for computing the threshold criteria and onset functions for both the large scale and the small scale precipitation, will likely undergo some further evolution. Some guidance as to how this should be done may be obtained by modelling arrays of convective elements. However, the most exciting avenue for future research could be a thorough exploration of the predictability aspects of the whole forecast problem. This could lead to the issuing of precipitation forecasts which give some estimation of the probable error along with the predicted amounts and types themselves.

## Acknowledgements

W. S. Creswick collaborated on the development of the baroclinic model. Some of the improvements in the precipitation scheme have arisen from fruitful and stimulating discussions with all past and present colleagues in Dynamic Prediction Research Division; others have come from the noting of specific deficiencies in the operational forecasts by R. Anderson, Head of the Analysis and Prognosis Unit, and his staff members.

Special thanks go to Y. R. G. Bourassa and Mrs C. Thibeault. Mr Bourassa looked after the systems aspects of the development work on the precipitation scheme, coded many of the computer programs, and drafted the figures. Mrs Thibeault coded the threat score verification procedures and some of the input and output programs.

## REFERENCES

Asselin, R. 1967. The operational solution of the balance equation. *Tellus 19*, 24–32.

Danard, M. B. 1964. On the influence of released latent heat on cyclone development. *J. Appl. Meteor. 3*, 27–37.

Danard, M. B. 1966*a*. A quasi-geostrophic numerical model incorporating effects of release of latent heat. *J. Appl. Meteor. 5*, 85–93.

Danard, M. B. 1966*b*. Further studies with a quasi-geostrophic numerical model incorporating effects of released latent heat. *J. Appl. Meteor. 5*, 388–395.

Davies, D. 1967. Three-layer numerical forecasts of precipitation amount. *Canadian Meteorological Memoirs 25*, 92 pp.

Davies, D. & Olson, M. P. 1968. Operational forecasts of 24-hour precipitation amount from the Central Analysis Office Computer. Canada Department of Transport, Meteorological Branch TEC. 670, 28 pp.

Davies, D. 1970. *Computations of tomorrow's rain.* Ph.D. Thesis, McGill University, Montreal, 485 pp.

Fulks, J. R. 1935. Rate of precipitation from adiabatically ascending air. *Mon. Wea. Rev. 63*, 291–294.

Godson, W. L. 1958. Atmospheric Thermodynamics. Canada Department of Transport, Meteorological Branch, special publication, 117 pp.

Harvey, R. 1969. Some experiments with telescoping grids in a baroclinic model. M.Sc. Thesis, McGill University, Montreal.

Kruger, H. B. 1965. A statistical dynamical objective analysis scheme. *Canadian Meteorological Memoirs 18*, 40 pp.

Kruger, H. B. & Asselin, R. J. M. 1967. A statistical dynamical objective analysis scheme: Supplement no. 1. *Canadian Meteorological Memoirs 23*, 38 pp.

Kruger, H. B. 1969. A statistical dynamical objective analysis scheme: Supplement no. 2. *Canadian Meteorological Memoirs 27*, 119 pp.

Kwizak, M. & Davies, D. 1969. Numerical forecasts of 24-hour precipitation amount. *Proceedings of the World Meteorological Organization International Union of Geodesy and Geophysics Symposium on Numerical Weather Prediction, Tokyo, 26 Nov.–4 Dec. 1968*, Meteorological Service of Japan, 10 pp.

Kwizak, M. & Robert, A. J. 1971. A semi-implicit scheme for grid point atmospheric models of the primitive equations. *Mon. Wea. Rev. 99*, 32–36.

Paulin, G. & Olson, M. P. 1972. Experiments with a four-level fine mesh baroclinic model. Canadian Meteorological Research Reports, 17 pp.

Robert, A. J. 1963. Baroclinic prediction experiments with a four-level statistical-dynamical model. *Canadian Meteorological Memoirs 15*, 32 pp.

Robert, A. J., Henderson, J. D. & Turnbull, C. C. 1972. An implicit time integration scheme for baroclinic models of the atmosphere. *Mon. Wea. Rev.*, 100, 329–335.

*Smithsonian Meteorological Tables* 1958. Rate of precipitation from adiabatically ascending air. Smithsonian Institute, Washington, D.C., pp. 325–326.

## ПРОГНОЗЫ ОСАДКОВ В КАНАДСКОМ МЕТЕОРОЛОГИЧЕСКОМ ЦЕНТРЕ

Оперативные прогнозы количества осадков осуществляются численной схемой, которая использует дефицит точки росы в качестве параметра влажности. Возникновение крупномасштабных осадков происходит постепенно и по мере того, как дефицит точки росы опускается ниже пороговой величины. Мелкомасштабные осадки разделены на несколько метеорологических компонентов, каждый из которых параметризуется отдельно. Недавно схема была улучшена путем уменьшения горизонтального интервала сетки с 381 до 190,5 *км*.